

Efficient resonance computations for Helmholtz problems based on a Dirichlet-to-Neumann map

Juan Carlos Araujo-Cabarcas¹, Christian Engström¹, Elias Jarlebring²

Abstract

We present an efficient procedure for computing resonances and resonant modes of Helmholtz problems posed in exterior domains. The problem is formulated as a nonlinear eigenvalue problem (NEP), where the nonlinearity arises from the use of a Dirichlet-to-Neumann map, which accounts for modeling unbounded domains. We consider a variational formulation and show that the spectrum consists of isolated eigenvalues of finite multiplicity that only can accumulate at infinity. The proposed method is based on a high order finite element discretization combined with a specialization of the Tensor Infinite Arnoldi method. Using Toeplitz matrices, we show how to specialize this method to our specific structure. In particular we introduce a pole cancellation technique in order to increase the radius of convergence for computation of eigenvalues that lie close to the poles of the matrix-valued function. The solution scheme can be applied to multiple resonators with a varying refractive index that is not necessarily piecewise constant. We present two test cases to show stability, performance and numerical accuracy of the method. In particular the use of a high order finite element discretization together with TIAR results in an efficient and reliable method to compute resonances.

Keywords:

Nonlinear eigenvalue problems, Helmholtz problem, scattering resonances, Dirichlet-to-Neumann map, Arnoldi's method, Bessel functions, Matrix functions

1. Introduction

In this paper we consider the numerical approximation of resonances in an open system, where the solutions satisfy the Helmholtz equation for a given refractive index $\eta(x)$. In general, resonances of an operator are defined as poles of the resolvent operator taken in a particular generalized sense [53, 38]. For Helmholtz equation Lenoir et al. [34] have shown that resonances are solutions to a nonlinear eigenvalue problem (NEP) with a Dirichlet-to-Neumann (DtN) map $\mathcal{G}(\lambda)$ on an artificial boundary Γ . The pair (u, λ) is a scattering resonance pair if

$$\begin{aligned} \Delta u + \lambda^2 \eta^2 u &= 0 & \text{in } \Omega, \\ \frac{\partial u}{\partial n} &= \mathcal{G}(\lambda)u & \text{on } \Gamma, \end{aligned} \tag{1}$$

¹Department of Mathematics and Mathematical Statistics, Umeå University, MIT-Huset, 90187 Umeå, Sweden

²Department of Mathematics, Royal Institute of Technology (KTH), Stockholm, SeRC Swedish e-Science Research Center

where $\partial u / \partial n$ is the normal derivative and the non-negative function $\eta^2 - 1$ has compact support contained in the open domain Ω . Hence, although our differential operator (1) is linear in λ^2 the DtN operator $\mathcal{G}(\lambda)$ (which we formalize in Section 2) depends in a nonlinear way on the eigenvalue λ . In this work we present a new computational approach for approximating resonances of (1) in an efficient and accurate way.

We present in Section 2.1 a variational formulation of the PDE (1) with the DtN map and show that the spectrum of the operator function consists of isolated eigenvalues of finite multiplicity, which accumulate only at infinity. This variational formulation is the base for the finite element method (FEM) in Section 3. In the FEM-implementation we discretize the operator function using high order Gauss-Lobatto shape functions and apply the p -version of the finite element method. The lower part of the spectrum of the operator function is then well approximated by the matrix function. Then very accurate approximations of the scattering resonance pairs are obtained if the nonlinear matrix eigenvalue problem can be solved accurately.

The considered NEP is of the type: find $\lambda \in \mathbb{C}$ in an open subset of the complex plane and a non-zero $u \in \mathbb{C}^n$ such that

$$T(\lambda)u = 0. \quad (2)$$

In our case T is meromorphic in \mathbb{C} , with poles in the region of interest defined as scaled roots of Hankel functions. Many numerical methods for the NEP (2) have been developed in the numerical linear algebra community, in particular when T is holomorphic in a large domain. Since the NEP with an arbitrary normalization is a system of nonlinear equations, Newton's method can be applied and considerably improved, e.g., by using block variations that can compute several eigenpairs simultaneously [33]. However, Newton-type methods bear the danger that some eigenvalues close to a given target could be missed.

There are also generalizations of successful methods for linear eigenvalue problems, e.g., the nonlinear Arnoldi method [50], the Jacobi-Davidson method [11] and LOBPCG [47]. Numerical methods for NEP can be based on contour integrals of the generalized resolvent $T^{-1}(\lambda)$ [2, 12, 18, 8, 25]. The DtN-map is the source of the complicated nonlinearity in the eigenvalue parameter λ . Several other problems have been approached with artificial boundary conditions and NEPs; see, e.g., the NEP arising in the modeling of an electromagnetic cavity [35], the model of an optical fiber in [31] and bi-periodic slabs [48]. There are also several approaches leading to NEPs developed in the context of photonic crystals [46, 19, 32, 16]. To our knowledge, none of the methods developed in those papers have been adapted to resonance problems of our type.

Our methods belong to a class of methods which can be interpreted as Krylov methods, either for an infinite-dimensional problem, or as a dynamically increasing companion linearization of an approximation of the problem [28, 9, 21]. For recent developments and problems see [51] and [10]. Our approach is based on the infinite Arnoldi (IAR) method [28]. In particular, we adapt the variant with a tensor representation of the basis presented in [27], called the tensor infinite Arnoldi method (TIAR). This method is designed to find all eigenvalues close to a given shift, where the radius of convergence depends on properties of the matrix-valued function (2). The infinite Arnoldi method (both IAR and TIAR) requires access a procedure to compute a quantity involving the derivatives of the problem. In Section 4 we derive an algorithm to compute the necessary quantities for our NEP which contains nonlinearities expressed as quotients of Hankel functions. In order to improve the convergence of the method, we introduce a pole cancellation technique which transforms the problem by removing poles.

In Section 5 we provide a characterization of the performance of our approach. In particular,

we show that the new infinite Arnoldi method together with a p -FEM strategy is an efficient and reliable tool for resonance calculations with the DtN map.

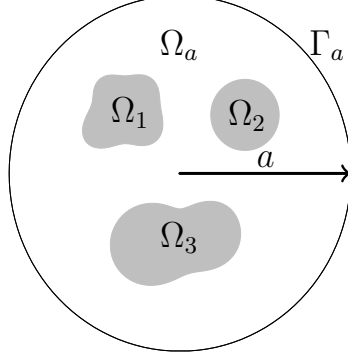


Figure 1: Example geometry of resonators Ω_i , $i = 1, 2, 3$ bounded by a circle.

2. Background and preliminaries

Results for the problem (1) can be found in a considerable amount of literature; see [42, 34, 15] and references therein. For $\text{Im } \lambda > 0$ we have uniqueness results [42, Chapter VIII] and resonance values are therefore in the region $\text{Im } \lambda < 0$.

Let $\Omega_a \subset \mathbb{R}^2$ be an open disk of radius a and boundary Γ_a . Assume $\eta \in L^\infty(\Omega_a)$ and that the non-negative function $\eta^2 - 1$ has compact support contained in Ω_a . A schematic setup of an example is illustrated in Figure 1. The resonance problem restricted to Ω_a is formally to find non-trivial solutions (u, λ) such that (1) holds, where

the DtN operator on the circle Γ_a has the explicit form

$$\mathcal{G}(\lambda)u := \frac{1}{2\pi} \sum_{\nu=-\infty}^{\infty} g_\nu(\lambda) e^{i\nu\theta} \int_0^{2\pi} u(a, \theta') e^{-i\nu\theta'} d\theta', \quad (3)$$

where

$$g_\nu(\lambda) := \lambda \frac{H'_\nu(\lambda a)}{H_\nu(\lambda a)} \quad (4)$$

and $\mathcal{G}(\lambda) : H^{1/2}(\Gamma_a) \rightarrow H^{-1/2}(\Gamma_a)$ is bounded [34]. In the following, we identify the dual pairing $\langle \cdot, \cdot \rangle_{H^{-1/2}(\Gamma_a) \times H^{1/2}(\Gamma_a)}$ with the L^2 -inner product $(\cdot, \cdot)_{\Gamma_a}$ over Γ_a . The theory presented in [34] can with minor changes be used in the present case to derive properties of a variational formulation of the problem.

2.1. Variational formulation

Let S denote the union of the set of zeros of $H_\nu(\lambda a)$, $\nu \in \mathbb{Z}$. The eigenvalues of (1) are determined by the following variational problem: Find $u \in H^1(\Omega_a) \setminus \{0\}$ and $\lambda \in \mathcal{D} := \mathbb{C} \setminus \{\mathbb{R}^- \cup S\}$ such that for all $v \in H^1(\Omega_a)$

$$(\nabla u, \nabla v)_{\Omega_a} - \lambda^2 (\eta^2 u, v)_{\Omega_a} - (\mathcal{G}(\lambda)u, v)_{\Gamma_a} = 0, \quad (5)$$

where $(u, v)_{\Omega_a} := \int_{\Omega_a} u \bar{v} dx$, $(\nabla u, \nabla v)_{\Omega_a} := \int_{\Omega_a} \nabla u \cdot \nabla \bar{v} dx$, and

$$(\mathcal{G}u, v)_{\Gamma_a} = \sum_{\nu=-\infty}^{\infty} \lambda a \frac{H'_\nu(\lambda a)}{H_\nu(\lambda a)} \hat{u}_\nu \bar{\hat{v}}_\nu, \quad \hat{\varphi}_\nu = \frac{1}{\sqrt{2\pi}} \int_0^{2\pi} \varphi(a, \theta') e^{-i\nu\theta'} d\theta'. \quad (6)$$

Let $(u, v)_1 := (\nabla u, \nabla v)_{\Omega_a} + (\eta^2 u, v)_{\Omega_a}$. Then the norm $\|u\|_1 := \sqrt{(u, u)_1}$ is equivalent to the standard norm on $H^1(\Omega_a)$. Define the operator $\mathcal{F}(\lambda) : H^1(\Omega_a) \rightarrow H^1(\Omega_a)$ by

$$(\mathcal{F}(\lambda)u, v)_1 := (\lambda^2 + 1)(\eta^2 u, v)_{\Omega_a} + (\mathcal{G}(\lambda)u, v)_{\Gamma_a}. \quad (7)$$

An operator formulation of (5) is to find $u \in H^1(\Omega_a) \setminus \{0\}$ and $\lambda \in \mathcal{D}$ such that

$$(I - \mathcal{F}(\lambda))u = 0. \quad (8)$$

Let $\mathcal{L}(H^1(\Omega_a))$ denote the space of bounded linear operators on $H^1(\Omega_a)$. An operator $A \in \mathcal{L}(H^1(\Omega_a))$ is Fredholm if it has finite-dimensional kernel $\ker A$ and cokernel $\text{coker } A$. The index of a Fredholm operator is $\text{ind } A := \dim \ker A - \dim \text{coker } A$. The essential spectrum of A denoted $\sigma_{\text{ess}}(A)$ is the set of complex numbers such that $A - \lambda I$ is not Fredholm. Let $\sigma_\infty(A) \subset \sigma_{\text{ess}}(A)$ denote the set of eigenvalues of infinite multiplicity.

Let $\mathcal{G}_{\nu_{\max}}(\lambda)$ denote the operator (3) truncated after $|\nu| = \nu_{\max}$ and let $I - \mathcal{F}_{\nu_{\max}}(\lambda)$, $\lambda \in \mathcal{D}$ denote the operator defined by

$$((I - \mathcal{F}_{\nu_{\max}}(\lambda))u, v)_1 := (u, v)_1 - (\lambda^2 + 1)(\eta^2 u, v)_{\Omega_a} - (\mathcal{G}_{\nu_{\max}}(\lambda)u, v)_{\Gamma_a}. \quad (9)$$

The operator function with a truncated DtN map (9) is the base for the numerical method and the following proposition shows that the spectrum is discrete with no finite accumulation point in the right-half plane.

Proposition 2.1. *Let $\nu_{\max} \in \{0, 1, \dots, \infty\}$. Then the $H^1(\Omega_a)$ -spectrum of the operator valued function $I - \mathcal{F}_{\nu_{\max}} : \mathcal{D} \rightarrow \mathcal{L}(H^1(\Omega_a))$ consists of isolated eigenvalues of finite multiplicity. Moreover, these eigenvalues can not have a finite accumulation point in the right-half plane.*

Proof. The function $\mathcal{F}_{\nu_{\max}} : \mathcal{D} \rightarrow \mathcal{L}(H^1(\Omega_a))$ is holomorphic [34, prop 4] and $I - \mathcal{F}_{\nu_{\max}}(\lambda)$ is a Fredholm operator of index zero [34, prop 5]. Moreover, we have

$$ia \frac{H'_\nu(ia)}{H_\nu(ia)} = a \frac{K'_\nu(a)}{K_\nu(a)}, \quad (10)$$

where $K_\nu(a) = \frac{\pi}{2} i^{\nu+1} H_\nu(ia)$, $\nu \in \mathbb{Z}$ are the modified Bessel functions [52]. The expression (10) is negative since $K_\nu(a) > 0$ and $K'_\nu(a) < 0$ for $a > 0$ [52, p. 181]. Hence $(\mathcal{G}_{\nu_{\max}}(i)u, u)_{\Gamma_a} < 0$ and

$$(u, u)_1 - (\mathcal{F}_{\nu_{\max}}(i)u, u)_1 = (u, u)_1 - (\mathcal{G}_{\nu_{\max}}(i)u, u)_{\Gamma_a} \geq \|u\|_1^2,$$

which shows that the resolvent set of $I - \mathcal{F}$ is non-empty. Hence, from the analytical Fredholm theorem follows that the spectrum is discrete and all eigenvalues are of finite multiplicity [20, Theorem 5.1]. In the right half-plane the eigenvalues can therefore only accumulate at the poles. The location of the poles is a function of a , but the spectrum is for large enough a independent of a , which implies that we have no accumulation in the right half-plane. \square

In Section 4.4, we improve convergence of the infinite Arnoldi method by multiplying the original matrix-valued function with a polynomial. In Proposition 2.2, we prove basic properties of the underlying operator-valued function. This proposition shows that the canceled poles will be in the essential spectrum of the modified operator.

Proposition 2.2. *Take $\mathcal{B} \subset \overline{\mathcal{D}}$ in the right-half plane such that \mathcal{F} has exactly one pole z in \mathcal{B} . Then is $\tilde{T}(\lambda) : H^1(\Omega_a) \rightarrow H^1(\Omega_a)$,*

$$\tilde{T}(\lambda) := (\lambda - z)I - \tilde{\mathcal{F}}(\lambda), \quad \tilde{\mathcal{F}}(\lambda) := (\lambda - z)\mathcal{F}(\lambda) \quad (11)$$

holomorphic in \mathcal{B} , $\{z\} = \sigma_{\text{ess}}(\tilde{T}) = \sigma_{\infty}(\tilde{T})$, and $\tilde{T}(z)$ is of rank one.

Proof. Take without loss of generality $a = 1$. Since all zeros of $H_{\nu}(\lambda)$ are simple [1, p 370], we have by definition $H_{\nu}(\lambda) = (\lambda - z)f(\lambda)$ with f holomorphic and $f(z) \neq 0$. Hence,

$$\frac{H'_{\nu}(\lambda)}{H_{\nu}(\lambda)} = \frac{1}{\lambda - z} + \frac{f'(\lambda)}{f(\lambda)},$$

which implies that \tilde{T} is holomorphic in \mathcal{B} . Since $H^1(\Omega_a)$ is infinite dimensional, it follows that $\tilde{T}(z)$ is not Fredholm. Assume $H_{\nu_z}(z) = 0$, $H_{\nu}(z) \neq 0$, $\nu \neq \nu_z$. Then $(\tilde{T}(z)u, v)_1 = -z\hat{u}_{\nu_z}\tilde{v}_{\nu_z}$, which implies that $\tilde{T}(z)$ and $\tilde{T}(z)^*$ are of rank one and hence $z \in \sigma_{\infty}(\tilde{T})$. \square

Remark 1. Proposition 2.2 shows that a pole z after multiplication by $\lambda - z$ is an eigenvalue of infinite multiplicity of the new operator function. This change of the spectral properties also apply more generally. Let H denote an infinite dimensional Hilbert space and assume that F is a $\mathcal{L}(H)$ -valued finitely meromorphic function at z . Hence,

$$F(\lambda) = \sum_{m=-s}^{\infty} (\lambda - z)^m F_m,$$

where $F_{-s}, F_{-s+1}, \dots, F_{-1}$ are finite rank. Define the bounded operator function

$$\tilde{T}(\lambda) := (\lambda - z)^s I - \tilde{\mathcal{F}}(\lambda), \quad \tilde{\mathcal{F}}(\lambda) := (\lambda - z)^s \mathcal{F}(\lambda). \quad (12)$$

Then $z \in \sigma_{\infty}(\tilde{T})$, since $\tilde{T}(z) = -F_{-s}$ is finite rank. However if F_{-s} is not finite rank, z will in general not be an eigenvalue of infinite multiplicity; see for example [18].

3. Discretization with the finite element method

The disk Ω_a , depicted in Figure 1, is covered with a regular and quasi uniform finite element mesh \mathcal{T} consisting of quadrilateral elements $\{K_i\}_{i=1}^N$. Let ρ_i be the diameter of the largest ball contained in K_i and denote by h the maximum mesh size $h := \max \rho_i$. Let \mathcal{P}_p denote the space of polynomials on \mathbb{R}^2 of degree $\leq p$ and set $\gamma := \{h, p\}$ [44, Ch 4]. We define the finite element space $S^{\gamma}(\Omega_a) := \{u \in H^1(\Omega_a) : u|_{K_i} \in \mathcal{P}_p(K_i) \text{ for } K_i \in \mathcal{T}\}$, and $N := \dim(S^{\gamma}(\Omega_a))$ [5]. Furthermore, all our computations are done in the approximated domain Ω_a^{γ} by using curvilinear elements following standard procedures [5].

From (5) we state the finite element problem: Find $u_{\gamma} \in S^{\gamma}(\Omega_a^{\gamma}) \setminus \{0\}$ and $\lambda_{\gamma} \in \mathcal{D}$ such that

$$(\nabla u_{\gamma}, \nabla v)_{\Omega_a^{\gamma}} - \lambda_{\gamma}^2 (\eta^2 u_{\gamma}, v)_{\Omega_a^{\gamma}} - (\mathcal{G}_{\nu_{\max}}(\lambda_{\gamma}) u_{\gamma}, v)_{\Gamma_a^{\gamma}} = 0 \text{ for all } v \in S^{\gamma}(\Omega_a^{\gamma}). \quad (13)$$

We showed in Section 2.1 that the analytic operator function $I - \mathcal{F}_{\nu_{\max}}$ with a truncated DtN map is Fredholm-valued on \mathcal{D} and that the resolvent set is non-empty. Hence, all eigenvalues are isolated and of finite multiplicity. Moreover, from Karma [29, 30] follows that any sequence $\{\lambda_\gamma\}$, $\dim S^\gamma(\Omega_a^\gamma) \rightarrow \infty$ of approximative eigenvalues of (13) converges to an eigenvalue λ of (5). The eigenfunctions are in $H^2(\Omega_a)$ and are piecewise analytic if the interfaces are analytic curves. Optimal convergence is expected under the assumptions that all interfaces are resolved by curvilinear cells and the eigenvalues are semi-simple. Hence, exponential convergence is expected with p -FEM and optimal converge rates are expected with h -FEM [4, 40].

3.1. Assembly of the FE matrices

Let $\{\varphi_1, \dots, \varphi_N\}$ be a basis of $S^\gamma(\Omega_a^\gamma)$. Then $u_\gamma \in S^\gamma(\Omega_a^\gamma)$ can be written in the form

$$u_\gamma = \sum_{j=1}^N \xi_j \varphi_j \quad (14)$$

and the entries in the finite element matrices are

$$A_{ij} = (\nabla \varphi_j, \nabla \varphi_i)_{\Omega_a^\gamma}, \quad M_{ij} = (\eta^2 \varphi_j, \varphi_i)_{\Omega_a^\gamma}, \quad G_{ij}(\lambda) = \sum_{\nu=-l}^l \lambda a \frac{H'_\nu(\lambda a)}{H_\nu(\lambda a)} Q_{ij}^\nu \quad (15)$$

with

$$Q_{ij}^\nu = \hat{\varphi}_j^\nu \bar{\varphi}_i^\nu, \quad \hat{\varphi}_j^\nu = \frac{1}{\sqrt{2\pi}} \int_0^{2\pi} \varphi_j(a, \theta') e^{-i\nu\theta'} d\theta', \quad i, j = 1, \dots, N. \quad (16)$$

The nonlinear matrix eigenvalue problem is then: Find the eigenpairs $(\lambda, \xi) \in \mathcal{D} \times \mathbb{C}^N \setminus \{0\}$ such that

$$T(\lambda) \xi := (A - \lambda^2 M - G(\lambda)) \xi = 0. \quad (17)$$

In the assembly routine, we only store the vectors $q_j^\nu = \hat{\varphi}_j^\nu$ and then compute the matrices as $Q^\nu = q^\nu \otimes \bar{q}^\nu$. Notice that $q_j^\nu = 0$ for nodes x_j such that $\text{supp}(\varphi_j) \cap \Gamma_a = \emptyset$. If the ordering of nodes is such that the N_a boundary nodes are placed first, then the Q^ν matrices have a dense upper-left block of size $N_a \times N_a$. This lost of sparsity is taken into account in the assembly routine, where we allow extra entries in the sparsity pattern of the FE matrices.

It is a standard technique to use Gauss-Legendre quadratures for the evaluation of integrals in FE. However, the trace integral (16) requires that the number of quadrature points is increased linearly with ν , because the integrand contains $e^{i\nu\theta(x_1, x_2)}$.

All numerical experiments have been carried out using the finite element library *deal.II* [7] with Gauss-Lobatto shape functions [45, Sec. 1.2.3]. For fast assembly and computations with complex numbers the package PETSc [6] is used.

The computational platform was provided by the High-Performance Computing Center North (HPC2N) at Umeå University, and all experiments were run on the distributed memory system Abisko. The jobs were run in serial on an exclusive node: during the process, no other jobs were running on the same node. Node specifications: four AMD Opteron 6238 processors with a total of 48 cores per node.

4. Specialization of the infinite Arnoldi method

Our algorithm for solving the NEP (17) is based on the tensor infinite Arnoldi method (TIAR) [27, Algorithm 2], which is an improvement of the infinite Arnoldi method (IAR) [28]. The version of the infinite Arnoldi method considered here can be viewed as the standard Arnoldi method applied to the companion linearization arising from a Taylor expansion of an analytic matrix-valued function T [28]. More precisely, it can be derived from a particular companion linearization of the Taylor expansion of T and Arnoldi's method for eigenvalue problems. The particular choice of companion linearization provides a structure such that the truncation parameter in a certain sense can be increased to infinity and the algorithm is therefore equivalent to Arnoldi's method applied to an infinite matrix.

Hence, the algorithm generates a Hessenberg matrix and the eigenvalues of this matrix correspond to eigenvalue approximations of the NEP.

TIAR is a variant of IAR where a tensor representation of the basis of IAR is used, which results in an algorithm of the same complexity as IAR but it requires less memory. Moreover, the usage of tensors in TIAR makes it considerably more efficient than IAR for certain types of problems [27] on modern computer architectures. We derive below a new version of TIAR adapted to the special structure of (17).

4.1. Quantities required for the infinite Arnoldi method

All of the variants of the infinite Arnoldi method require (in some way) access to derivatives. In TIAR we need a procedure to compute

$$x_0 = -T(\mu)^{-1} \left(\sum_{i=1}^k T^{(i)}(\mu) x_i \right), \quad (18)$$

where k is the iteration count, and we compute eigenvalues close to a target μ .

The matrix $T(\mu)$ is independent of k and we compute an LU-factorization of $T(\mu)$ before starting the iterations in TIAR. Without loss of generality, we write T of the form

$$T(\lambda) = \sum_{j=1}^N A_j f_j(\lambda). \quad (19)$$

Then, we express the NEP (17) in the form (19) with

$$A_1 = A, \quad f_1(\lambda) = 1 \quad (20a)$$

$$A_2 = M, \quad f_2(\lambda) = -\lambda^2 \quad (20b)$$

and for $j = 3, \dots, 2\nu_{\max} + 3$,

$$A_j = -aq_{j-\nu_{\max}-3} q_{j-\nu_{\max}-3}^T \quad (21a)$$

$$f_j(\lambda) = g_{j-\nu_{\max}-3}(\lambda) = \frac{H'_{j-\nu_{\max}-3}(a\lambda)}{H_{j-\nu_{\max}-3}(a\lambda)} \lambda. \quad (21b)$$

Hence, (18) for the problem stated in (17) can be written as

$$x_0 = -T(\mu)^{-1} \left(\sum_{j=1}^{2\nu_{\max}+3} A_j \sum_{i=1}^k x_i f_j^{(i)}(\mu) \right). \quad (22)$$

In order to specialize TIAR to the considered NEP a procedure to compute the derivatives in (22) is required.

4.2. High-order quotient and products rules with Toeplitz matrices

The nonlinearities (21b) are products and quotients of analytic functions of the form

$$g(\lambda) = \frac{h_1(\lambda)}{h_2(\lambda)} p(\lambda), \quad (23)$$

where h_1 and h_2 are analytic functions and p a polynomial. Formula (22) includes (high-order) derivatives of such scalar functions. There are high-order product and quotient rules for differentiation, which are explicit and lead to formulas for the high-order derivatives of (23). However, the direct application of the high-order product and quotient rules, i.e., the general Leibniz rule, are somewhat unsatisfactory in terms of computation time. Here we propose to use a formula involving Toeplitz matrices, and compute directly a given number of derivatives using only matrix-vector operations.

The derivation of our Toeplitz matrix computational formula for the derivatives, can be done by comparing terms in a Taylor expansion of $g(\lambda)$. For our purposes it is more natural to use matrix functions in the sense of [23]. Let J_μ denote a Jordan matrix with eigenvalue μ ,

$$J_\mu = \begin{bmatrix} \mu & 1 & & \\ & \ddots & \ddots & \\ & & \ddots & 1 \\ & & & \mu \end{bmatrix}. \quad (24)$$

The matrix function of a Jordan matrix is a triangular Toeplitz matrix [23, Definition 1.2] containing scaled derivatives of the scalar function,

$$f(J_\mu^T) = f(J_\mu)^T = \begin{bmatrix} \frac{f(\mu)}{0!} & & \\ \vdots & \ddots & \\ \frac{f^{(p-1)}(\mu)}{(p-1)!} & \cdots & \frac{f(\mu)}{0!} \end{bmatrix}. \quad (25)$$

Therefore, the derivatives of a function for which the corresponding matrix function is available can be computed with the formula

$$\begin{bmatrix} f(\mu) \\ f'(\mu) \\ \vdots \\ f^{(p-1)}(\mu) \end{bmatrix} = \text{diag}(u) f(J_\mu^T) e_1, \quad (26)$$

where $u^T = [0!, \dots, (p-1)!]$. Then, using formula (26), we find that the derivatives (23) are given by

$$\begin{bmatrix} g(\mu) \\ g'(\mu) \\ \vdots \\ g^{(p-1)}(\mu) \end{bmatrix} = \text{diag}(u) h_1(J_\mu^T) h_2(J_\mu^T)^{-1} p(J_\mu^T) e_1. \quad (27)$$

The TIAR algorithm can be applied to any NEP expressed in the form (19) for which efficient and reliable computation of the corresponding matrix function is available. Such matrix function representation is analogous to the input for several other methods and software packages, e.g., the block Newton method [33] and NLEIGS [21]. This representation is suitable for many NEPs including the problem considered in this paper (due to the derivative computation specialization provided here), but not in general for NEPs where the number of terms is large. Completely analogous to scalar-valued functions, products and quotients of matrix functions are expressed as matrix multiplies and inverses (which is formally a consequence of [23, Theorem 1.15]).

4.3. Derivative computations of Hankel functions

For the purpose of using formula (27), we require the matrix functions corresponding to (20) and (21b). These matrix functions are $f_1(S) = I$, $f_2(S) = -S^2$, and

$$f_j(S) = g_{j-\nu_{\max}-3}(S) = H'_{j-\nu_{\max}-3}(aS)H_{j-\nu_{\max}-3}(aS)^{-1}S, \quad j = 3, \dots, 2\nu_{\max} + 3. \quad (28)$$

The matrix function (28) could be computed directly if robust and efficient methods for matrix Hankel functions were available. To the best of our knowledge, there are unfortunately no such specialized methods.

Rather than computing the matrix function of the Hankel function explicitly, we use that for applying (27) only the matrix function of a transposed Jordan block is required. Hence, we compute the Toeplitz matrix (25) consisting of scaled derivatives. Then, the derivatives of the Hankel function can be robustly computed as follows. For notational convenience, let for any $r \in \mathbb{N}$,

$$\underline{H}_r(z) := [H_0(z), H_1(z), \dots, H_{r-1}(z)]^T \quad (29a)$$

$$\underline{H}_{-r}(z) := [H_0(z), H_{-1}(z), \dots, H_{1-r}(z)]^T \quad (29b)$$

$$= D_r \underline{H}_r(z), \quad (29c)$$

where $D_r = \text{diag}(1, -1, 1, -1, \dots) \in \mathbb{R}^r$ and (29c) follows from the symmetry of Hankel functions. Using the recursion formulas for Hankel functions, the infinite vector of derivatives of the Hankel functions can be written as

$$\underline{H}'_{\infty}(z) = B_{\infty} \underline{H}_{\infty}(z) \quad (30)$$

where B_{∞} is given by the infinite extension of a matrix B_r formed by the sum of a Toeplitz matrix and a rank-one matrix,

$$B_r = \begin{bmatrix} 0 & -1 & & & \\ 1/2 & \ddots & -1/2 & & \\ & \ddots & \ddots & \ddots & \\ & & 1/2 & \ddots & -1/2 \\ & & & 1/2 & 0 \end{bmatrix} \in \mathbb{R}^{r \times r}. \quad (31)$$

The relation (30) leads to a procedure to compute the derivatives summarized in the following lemma.

Lemma 2 (Hankel function derivative recursions). *Let the vector of Hankel functions be defined by (29) and the tridiagonal matrix B_r in (31). Then, the k th derivatives of Hankel functions are given by*

$$\frac{d^k}{dz^k} \underline{H}_r(az) = a^k [I_r, 0, \dots, 0] B_{r+k}^k \underline{H}_{r+k}(az) \quad (32)$$

and $\underline{H}_{-r}^{(k)}(z) = D_r \underline{H}_r^{(k)}(z)$.

Proof. By the chain rule and repeated application of (30) we have for an arbitrary derivative k ,

$$\frac{d^k}{dz^k} \underline{H}_\infty(az) = a^k \underline{H}_\infty^{(k)}(az) = a^k B_\infty^k \underline{H}_\infty(az).$$

The matrix B_∞ is tridiagonal. Therefore,

$$[I_r, 0, \dots] B_\infty^k = [I_r, 0, \dots, 0] [B_{k+r}^k, 0, \dots, 0]. \quad (33)$$

Then (32) follows from (33) with

$$\underline{H}_r^{(k)}(z) = [I_r, 0, \dots, 0] \underline{H}_\infty^{(k)}(z) = [I_r, 0, \dots, 0] B_\infty^k \underline{H}_\infty(z).$$

□

Remark 3 (Alternative ways to compute derivatives of Hankel functions). *There are in principle, many ways to numerically compute derivatives of Hankel functions, e.g., with various discretization schemes. An advantage of our approach is that it is exact in exact arithmetic, and appears relatively insensitive to round-off errors. We describe in Algorithm 1 how the computation can be performed with only matrix-vector products. This is easily integrated with the pole cancellation technique described in Section 4.4, and the large number of derivatives required in TIAR.*

4.4. Pole cancellation and derivative computation algorithm

Lemma 2 does provide a procedure to compute derivatives of the Hankel functions and it can be directly used to specialize TIAR to (17). We show in Section 5 that the direct application of the method numerically works well for some regions of the complex plane, but unfortunately not for the entire complex plane. The infinite Arnoldi method is designed for problems which are analytic in a large domain, and convergence cannot be guaranteed for eigenvalues outside the convergence disk for the power series expansion at μ . Below, use a transformation of the matrix function to increase the convergence radius by effectively cancelling poles. A similar holomorphic extension was successfully applied to a matrix-valued function that is used to determine surface waves in soil mechanics [49, Section 7.3.1]. Suppose $z_i, i = 1, \dots, p$ are zeros of Hankel functions and define

$$\tilde{T}(\lambda) := (\lambda - z_1) \cdots (\lambda - z_p) T(\lambda).$$

From Proposition 2.2 follows that \tilde{T} is holomorphic in a domain containing $z_i, i = 1, \dots, p$. Hence, we have a decomposition analogous to (19) where $\tilde{T}(\lambda) = \sum_i^N A_i \tilde{f}_i(\lambda)$, with

$$\tilde{f}_i(\lambda) := (\lambda - z_1) \cdots (\lambda - z_p) f_i(\lambda).$$

Note that the nonlinear terms of \tilde{T} are $\tilde{g}_m(\lambda) = (\lambda - z_1) \cdots (\lambda - z_p) g_m(\lambda)$, $m = -\nu_{\max}, \dots, m$, which are terms of the form (23) with $p(\lambda) := (\lambda_1 - z_1) \cdots (\lambda_1 - z_p) \lambda$. Therefore, we can still

use formula (27). By construction, the nonlinear (matrix) eigenvalue problem associated with \tilde{T} has the same solutions as the NEP associated with T , except for possibly $\lambda = z_i$. Moreover, the singularity set of \tilde{T} is the same as T except that z_1, \dots, z_p are not poles of \tilde{T} . The values $\lambda = z_i$ are not solutions to the NEP T , since z_i is a pole. However, Proposition 2.2 shows that the poles of the original operator function are eigenvalues of infinite multiplicity of the operator function obtained by multiplying with a polynomial. The matrix function \tilde{T} will then numerically have several additional eigenvalues close to the poles compared to the eigenvalues of T . It is therefore essential that an estimate of the quality of a computed eigenpair of \tilde{T} is based on the original matrix function T . In Section 5, we estimate the quality of a computed eigenpair by the standard backward error estimate (consistent e.g. with [36]) for NEPs

$$\|T(\lambda)v\|/\alpha(\lambda, v), \text{ with } \alpha(\lambda, v) := \|A\| + |\lambda|^2\|M\| + \sum_{\nu=-l}^l |\lambda|a|H'_\nu(a\lambda)|/|H_\nu(a\lambda)|\|Q^\nu\|.$$

We summarize the combination of (27) with the Hankel function derivative computation in Lemma 2 in Algorithm 1. In the algorithm we have taken advantage of the structure of the numerator and denominator in (23), and that the derivatives corresponding to all needed indexes can be computed simultaneously. The output of the algorithm is the matrix consisting of derivatives of \tilde{g}_i ,

$$X = \begin{bmatrix} x_1 & \cdots & x_{\nu_{\max}+1} \end{bmatrix} = \begin{bmatrix} \tilde{g}_0^{(0)} & \cdots & \tilde{g}_{\nu_{\max}}^{(0)} \\ \vdots & & \vdots \\ \tilde{g}_0^{(k_{\max})} & \cdots & \tilde{g}_{\nu_{\max}}^{(k_{\max})} \end{bmatrix}. \quad (34)$$

Note that $\tilde{g}_i = \tilde{g}_{-i}$ such that we can use (34) also for negative index.

Remark 4. *Efficiency improvements and memory requirements. Some further improvements in the computation of x_0 were achieved by also using the localization of the vectors q_i . More precisely, for $i > p + 2$ the contribution of A_1 and A_2 do not need to be taken into account. Note that in order to carry out m steps of TIAR for a NEP of size N , we mainly need to store a complex basis matrix of size $N \times m$. Hence, in our setting the memory required by TIAR is far less demanding than the storage required for the LU-factorization used for performing the initial step in (22).*

5. Numerical simulations

In the numerical computations, we discretize (5) with a finite element method and consider two geometries with smooth interfaces. Then we approximate the eigenvalues of the matrix problem (17) with the new version of TIAR outlined in Section 4. Note that in order to preserve the accuracy for basis functions of degree larger than one it is, for the considered geometries, mandatory to use curvilinear elements [14, 13]. When the eigenvalues are semi-simple, we expect optimal convergence with the h -version and with the p -version of the finite element method [3]. In h -FEM, we fix the polynomial order p of the basis functions and decrease the maximum size of the cells h . Then, the optimal convergence is algebraic:

$$\left| \frac{\lambda_j - \lambda_j^\gamma}{\lambda_j} \right| \leq cN^{-p}, \quad c > 0, \quad (35)$$

Algorithm 1: Derivative computation for (34)

input : Number of derivatives k_{\max} , largest index in modulus ν_{\max} , sequence of poles z_1, \dots, z_p

output: The matrix X in (34) consisting of derivatives of \tilde{g}_i

- 1 Compute $r_0 = \underline{H}_{k_{\max}+\nu_{\max}+1}(\mu) \in \mathbb{C}^{k_{\max}+\nu_{\max}+1}$ with (29)
- for** $k = 1, \dots, k_{\max} + 1$ **do**
- 2 | Compute $r_k = aB_{k_{\max}+\nu_{\max}}r_{k-1}$ where $B_{k_{\max}+\nu_{\max}+1}$ is given by (31)
- end**
- 3 Set $q = J^T e_1$ where $J = J_\mu \in \mathbb{C}^{k_{\max} \times k_{\max}}$ given in (24)
- for** $i = 1, \dots, p$ **do**
- 4 | Set $q = J^T q - z_i q$
- end**
- for** $i = 1, \dots, \nu_{\max} + 1$ **do**
- 5 | Compute the tridiagonal Toeplitz matrix $H \in \mathbb{C}^{k_{\max} \times k_{\max}}$ with (25) where we set $f^{(j)}(\mu) := (r_j)_i, j = 0, \dots, k_{\max}$
- 6 | Compute the tridiagonal Toeplitz matrix $H' \in \mathbb{C}^{k_{\max} \times k_{\max}}$ with (25) where we set $f^{(j)}(\mu) := (r_{j+1})_i, j = 0, \dots, k_{\max}$
- 7 | Set $x_i = H' H^{-1} q$
- end**

j	m	$\Re \lambda_j$	$\Im \lambda_j$	j	m	$\Re \lambda_j$	$\Im \lambda_j$
1	1	9.021 766 303 207	-0.273 829 280 623	4	0	19.243 876 046 899	-0.274 713 999 601
2	8	8.936 779 164 355	-0.164 935 525 246	5	19	19.241 527 655 113	-0.104 420 737 352
3	14	8.783 835 782 061	-0.000 247 588 219	6	25	19.156 200 970 821	-0.000 653 924 318

Table 1: *Selected reference eigenvalues for the problem 5.1, computed from (37) and ordered by $|\Im \lambda_j|$.*

where N denotes the number of degrees of freedom. In p -FEM, we fix the mesh and increase p , which result in the exponential rate of convergence

$$\left| \frac{\lambda_j - \lambda_j^\gamma}{\lambda_j} \right| \leq \alpha e^{-\beta N^{\frac{1}{2}}}, \quad \alpha, \beta > 0. \quad (36)$$

It is well known that hp -FEM (p -FEM in the case of smooth interfaces) is superior to h -FEM in terms of accuracy vs number of degrees of freedom [44] but the use of higher order basis functions results in less sparse matrices. Therefore, it is for a given matrix size more time consuming to solve a matrix eigenvalue problem generated by a high-order finite element method. The studied NEPs are solved with the specialization of the infinite Arnoldi method outlined in Section 4. We illustrate the convergence of the finite element method as well as the performance of the linear algebra solver. In particular, we show that a discretization with the p -version of the finite element method outlined in Section 3 together with the new version of the infinite Arnoldi method is an efficient tool for resonance calculations.

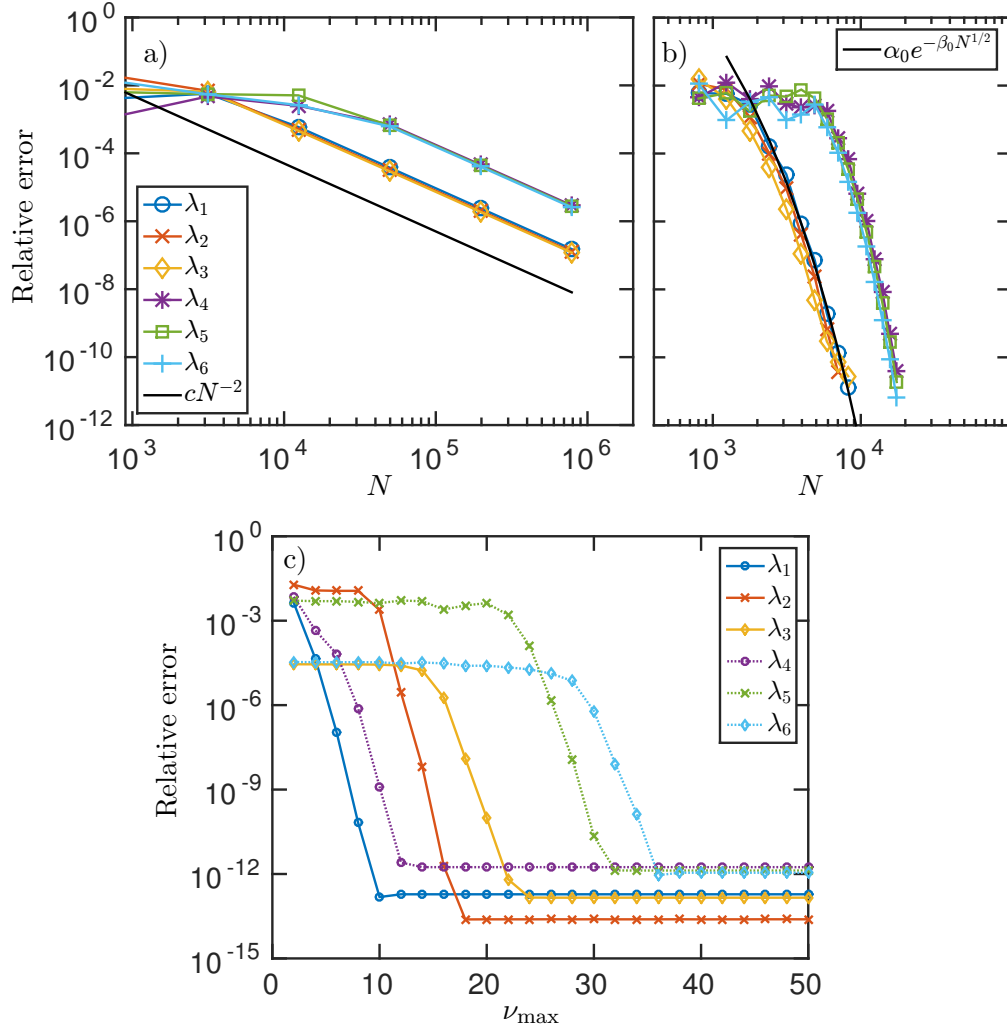


Figure 2: Convergence for problem 5.1: a) h -FEM with $p = 2$ and b) p -FEM with fitting curve (black): $\alpha_0 = 1.22 \times 10^5, \beta_0 = 0.4081$. c) convergence with respect to ν_{\max} .

j	$\text{Re } \lambda_j$	$\text{Im } \lambda_j$	j	$\text{Re } \lambda_j$	$\text{Im } \lambda_j$
1	3.499 842	-8.400 318 9	15	19.256 306 448 9	-0.066 528 956 84
2	3.082 426	-8.179 510 2	16	99.070 609 128 9	-0.533 898 079 75
3	3.662 856 165	-4.980 016 551	17	98.696 799 709 9	-0.386 922 639 003
4	3.035 882 038	-4.910 209 072	18	98.835 675 963 6	-0.069 143 373 791
5	1.098 616 611 0	-1.005 745 095 69	19	98.825 451 610 5	-0.059 689 390 790
6	2.165 520 379 3	-0.537 312 290 13	20	99.406 192 996 6	-0.000 006 880 063
7	4.370 036 082 6	-1.526 561 686 26	21	99.406 192 346 6	-0.000 006 849 959
8	3.958 068 685 7	-0.528 959 556 45	22	99.406 192 109 7	-0.000 009 251 593
9	4.894 990 528 7	-0.402 810 837 17	23	99.406 194 108 9	-0.000 009 059 285
10	20.001 865 223 0	-1.199 793 327 65	24	99.253 077 460 0	-0.000 000 004 940
11	19.159 017 340 2	-0.631 617 902 52	25	99.253 077 462 6	-0.000 000 004 465
12	20.329 616 908 4	-0.530 465 014 38	26	99.253 077 459 3	-0.000 000 004 441
13	21.059 617 919 8	-0.413 472 666 47	27	99.253 077 463 7	-0.000 000 004 263
14	19.176 565 085 7	-0.084 153 047 32	28	99.222 941 196 1	-0.000 000 000 000 1

Table 2: Reference eigenvalues for problem 5.2, computed with $p = 30$, $N=317\,281$.

5.1. Single disk problem

In this subsection, we consider the classical dielectric disk resonator [17]. Using separation of variables, we obtain equation (37). A complex Newton root finder is used to compute very accurate approximations of the resonances. These approximations are used as a benchmark for studying the convergence of the used finite element methods together with the new version of the infinite Arnoldi method.

Consider an open disk Ω_R with radius R and refractive index $\eta(r) = \eta_s$ in Ω_R and $\eta(r) = 1$ in $\Omega_R^+ := \mathbb{R}^2 \setminus \overline{\Omega}_R$. Exact solutions to this problem are given in [17] and the resonance relationship reads

$$J_m(\lambda\eta_s R)(H_m^{(1)}(\lambda R))' - \eta_s J_m'(\lambda\eta_s R)H_m^{(1)}(\lambda R) = 0. \quad (37)$$

For each m in equation (37), we search numerically n resonances $\lambda_{m1}, \dots, \lambda_{mn}$. The Newton root finder presented in [37] is used with machine precision stopping criterion.

In Table 1, we list a selection of benchmark values λ_{mn} computed from (37), which are used to evaluate accuracy and convergence of the numerical solutions.

The solutions λ_{mn} are classified as *external resonances* or *internal resonances* [17]. The internal resonances, also called *Whispering Gallery Modes* (WGM), have broad applications in optics, photonics, communications, and engineering [26]. These resonances feature negative imaginary parts that are close to the real axis. Approximation of the internal modes with FEM require that the oscillatory behavior inside the resonator is resolved, but the modes outside the resonator are almost constant and therefore less demanding to approximate.

Exterior resonances are characterized by having large negative imaginary parts and the corresponding modes grow very quickly outside the resonator. Hence, FEM approximation of these modes is demanding.

5.1.1. Approximation with FEM and TIAR

If the DtN map (3) is placed at $a = R$, then only one term is non-zero because the DtN map coincides with the compatibility condition for derivatives. However, by shifting the disk Ω_R a

distance d away from the origin and taking $a > R + d$, the radial symmetry is lost and more terms are necessary in the DtN map (3). This more demanding problem formulation is used to test our solution scheme in terms of accuracy as well as convergence with respect to the number of DtN terms. Let $\Gamma_a := \partial\Omega_a$ denote a circle of radius a centred in the origin and let $\Omega_R^d \subset \Omega_a$ denote the shifted disk. We choose $R = 1$ with the shifting distance $d = R/2$ along the x -axis, $\eta_s = 2$, and $a = 2$.

Once the geometry is set, we discretize (5) with the finite element method outlined in Section 3.1 and apply the new specialization of TIAR in Section 4 to a FE discretization with $p = 20$, $a = 2$ and $N = 19361$. In the TIAR scheme we use the shifts $\mu = 9 - 0.1i$ to approximate $\lambda_1, \lambda_2, \lambda_3$ and $\mu = 19 - 0.1i$ for $\lambda_4, \lambda_5, \lambda_6$, where $\lambda_1, \dots, \lambda_6$ are the reference values in Table 1. The resonances λ_3 and λ_6 are classified as interior resonances while the remaining values are classified as exterior resonances [17]. For the given shifts, we compute simultaneously approximations to both types of resonances. Hence, the used finite element space must be able to capture oscillations in the interior of the resonator and rapid growth in the exterior.

Figure 2 illustrates the convergence of a sequence of eigenvalues λ_j^γ approaching the reference values λ_j in Table 1. Optimal convergence rates are reached: (35) in a) and (36) in b). For the analysis of the ν_{\max} -dependence we work with a fixed discretization and plot in Figure 2 (c) relative errors vs ν_{\max} . We observe a preasymptotic phase until a critical $\nu_{\max} = \tilde{\nu}$ is reached and for $\nu_{\max} > \tilde{\nu}$ the convergence is very rapid. Figure 2 (c) also illustrates stability of TIAR in the sense that having more ν terms than $\tilde{\nu}$ in the numerical experiments did not result in larger numerical errors.

As expected, errors in the approximations λ_j^γ drop faster when λ_j in Table 1 correspond to an eigenvalue with small m . The empirical rule $\nu_{\max} > a\lambda$ was used in [22] as an estimate of the necessary number of truncation terms ν_{\max} in the DtN method applied for source problems ($\lambda \in \mathbb{R}$). Our computations indicate that $\nu_{\max} > a \operatorname{Re} \lambda$ can be used for the current eigenvalue problem. For example, from Figure 2 (c), it is clear that the relative errors of the numerical λ_j^γ decrease below 10^{-9} for $\nu_{\max} > a \operatorname{Re} \lambda_j^\gamma$.

5.2. Disk dimer problem

Adjacent resonators are of particular interest as they exhibit oscillatory modes that cannot be excited by single resonators and have interesting physical properties such as special mode symmetries (fanoresonances) that may exhibit strong coupling, and higher Q -factors [24, 41, 39].

The studied geometry consists of two disks of radius $R = 1/4$ separated vertically by a distance $s = R$. Each disk has constant refractive index $\eta = 2$, and are surrounded by vacuum $\eta = 1$. The setting is such that $\operatorname{supp}(\eta^2 - 1) \subset \Omega_a$ with $a = 1$. We study convergence by computing reference eigenvalues λ_j with the new specialization of TIAR, outlined in section 4, applied to a discretization with $p = 30$ and list them in Table 2.

Since no exact solution is available, we study convergence with respect to three different parameters: degrees of freedom N , ν and TIAR iterations k .

5.3. Approximation with FEM and TIAR

In Figure 4 we show convergence for the disk dimer problem. In (a) and (b) convergence with respect to N and in c) convergence with respect to ν . The computed relative errors of the eigenvalues satisfy the estimates (35) and (36). Hence, the numerical computation indicate that the asymptotic convergence rates are optimal. As expected, the preasymptotic phase is longer for

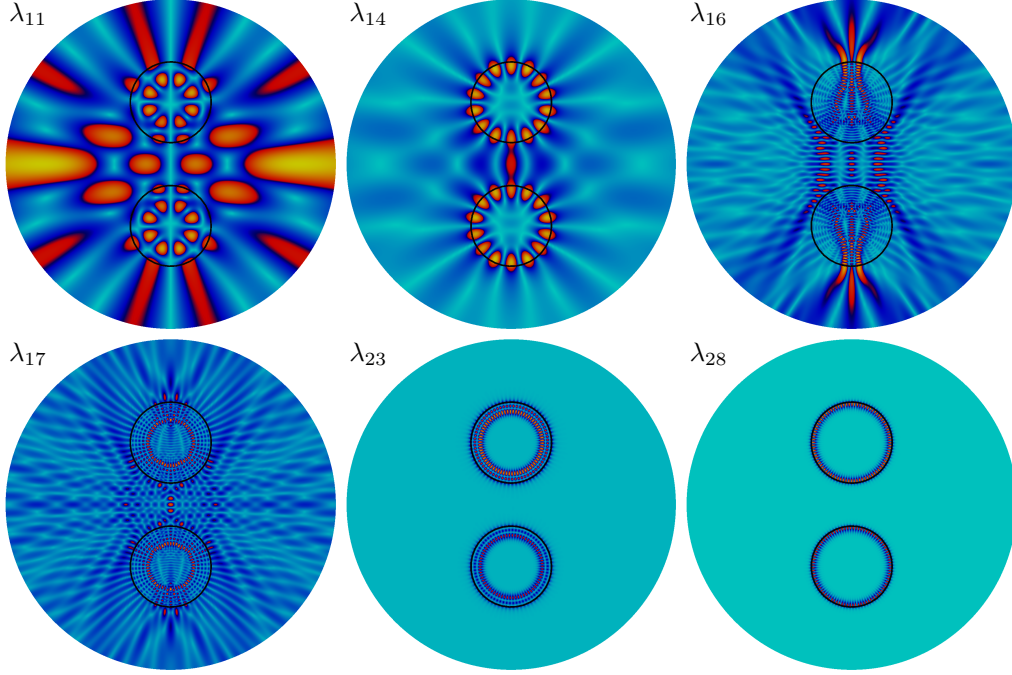


Figure 3: Fields $|u_j(x_1, x_2)|$ corresponding to eigenvalues λ_j given with bold font in Table 2.

large $\text{Re } \lambda_j$ [43] and eigenvalues with smaller $\text{Re } \lambda_j$ converge faster. This can be seen by comparing the model (36) for different λ_j^γ . The fitted curves following λ_{11}^γ and λ_{17}^γ are plotted in dashed-black and solid-black lines in Figure 4 (b). The exponential rate for λ_{11} is $\beta_1 = 0.1799$ and for λ_{17} is $\beta_2 = 0.1203$, then $\beta_1 > \beta_2$ is in agreement with $\text{Re } \lambda_{11} = 19.159 < \text{Re } \lambda_{17} = 98.697$.

The convergence of relative error with respect to ν_{\max} behaves similarly as described in Section 5.1. In Figure 4 (c), the real part of λ_{11} is 19.159 and the relative error drops below 10^{-8} for $\nu_{\max} > 20$. Similarly for $\text{Re } \lambda_{16} = 99.0706$, the relative error is below 10^{-10} for all $\nu_{\max} > 80$.

Figure 3 shows that the function u_{28} corresponding to λ_{28} oscillates in a confined region around the resonator resembling WGMs [26]. Furthermore, the figure shows that $|u_{28}(x)| \approx \text{constant}$ for $x \in \Gamma_a$. Hence, in the Fourier series (16) only the $\nu = 0$ term is necessary to accurately approximate u_{28} . In agreement, Figure 4 (c) shows that the relative error in λ_{28} is approximately 10^{-9} for $\nu_{\max} \geq 0$.

In Figure 5 (a) we present a selection of computed eigenvalues of equation (17) corresponding to the disk dimer problem. The eigenvalues marked with red stars are listed in Table 2. The blue bullets correspond to the poles z_j of $G(\lambda)$ defined in (15) with $a = 1$. In the Figure 5 (b) we illustrate a situation with $a = 2$, where there are poles in between the shift μ and the closest λ_j^γ . In this case a pole gets very close to λ_5 as illustrated in the Figure 5 (b). We evaluate the effectiveness of the pole cancellation technique by choosing $\mu = 1.15 - 0.8i$ and running TIAR with and without pole cancellation. In Figure 6 (b) we show the convergence vs. iterations of the experiment described above. Without pole cancellation we only get convergence for λ_5 (red dashed line), until stagnation at around 10^{-5} . When using pole cancellation, $\hat{\lambda}_5$ converges until machine precision (solid line) and $\tilde{\lambda}_6$ also converges (dotted line), which suggests that the radius of convergence is greater when pole cancellation is used.

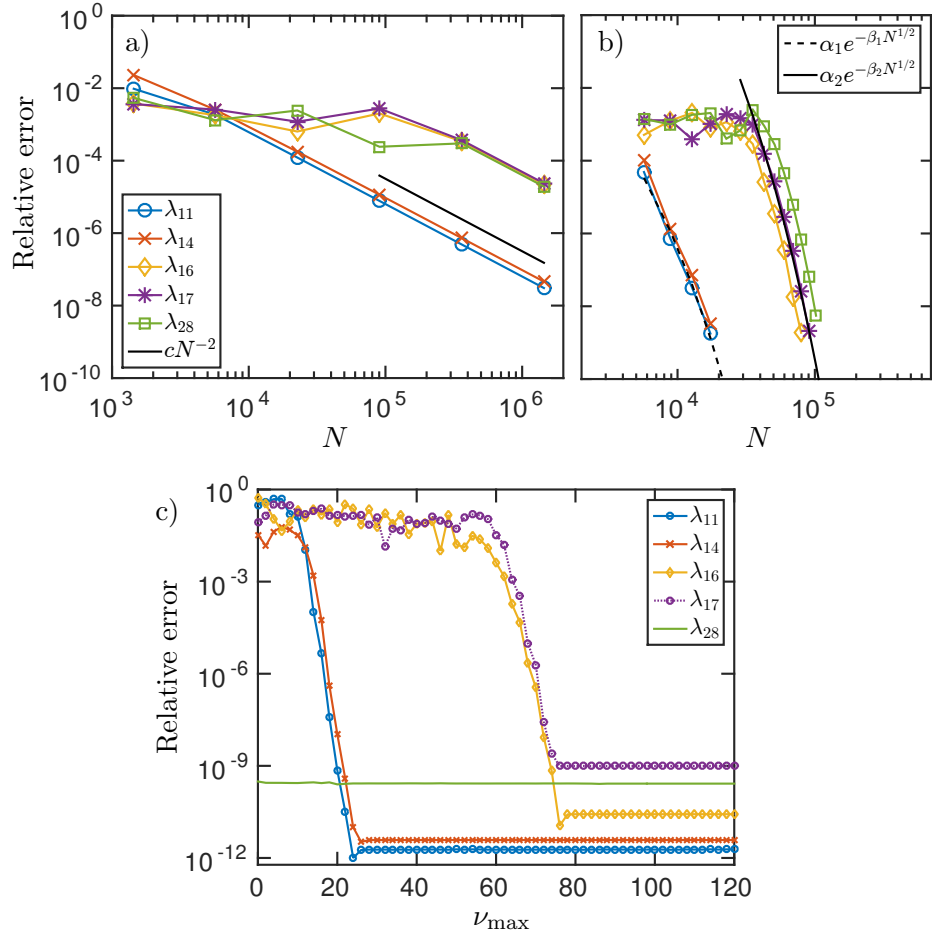


Figure 4: Convergence for problem 5.2: a) h-FEM with $p = 2$ and b) p-FEM. The fitting curves in black use: $\alpha_1 = 26.46, \beta_1 = 0.1799, \alpha_2 = 1.14 \times 10^7, \beta_2 = 0.1203$. c) convergence with respect to ν_{\max} .

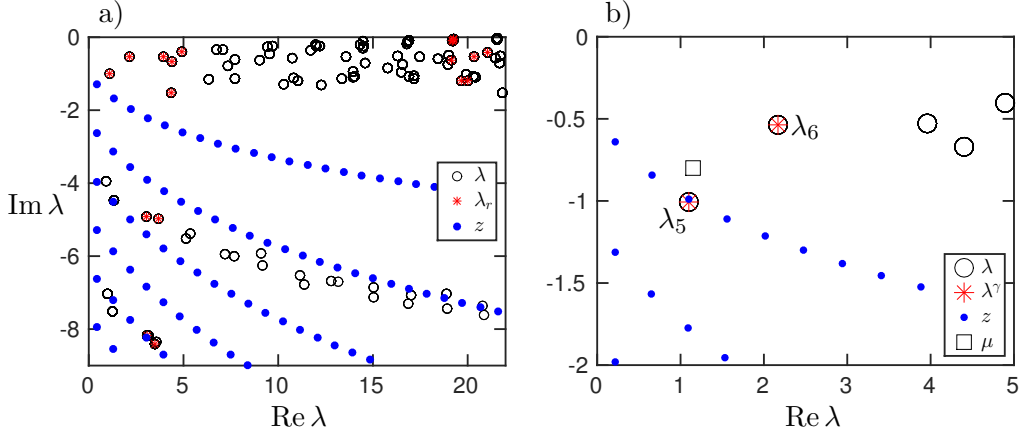


Figure 5: a) Eigenvalues λ computed with several shifts μ and $a = 1$. Selected reference eigenvalues λ_r , included in Table 2, are marked with red stars and poles z in blue bullets. b) Situation illustrating pole cancellation with $a = 2$.

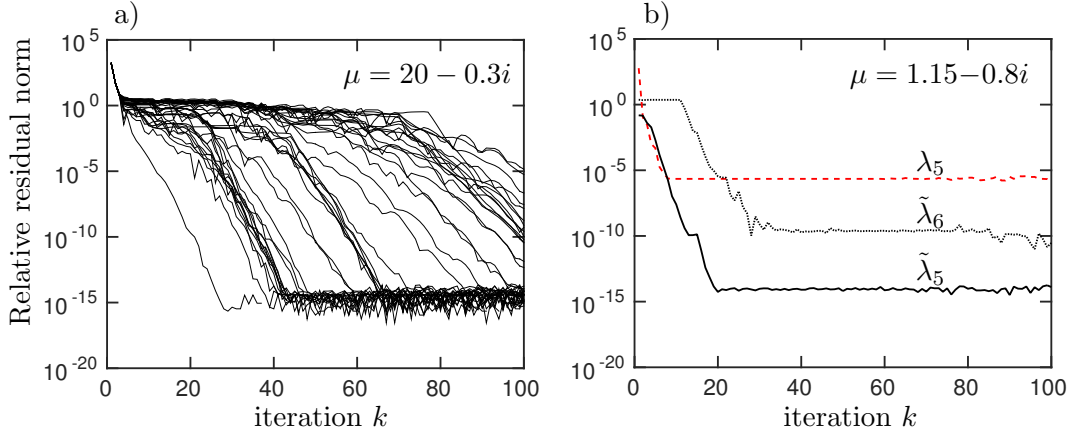


Figure 6: a) TIAR eigenvalue convergence vs iterations. b) Case illustrating Pole cancellation. We show convergence without pole canceling in red dashed line and convergence using pole canceling in solid line.

Performance comparison: Below we briefly discuss the performance of the proposed NEP solver. In the startup phase, we compute for given shift μ the LU factorization of $T(\mu)$ and refer to the time spent as LU time. The LU factorization is only computed once and it is used in the inverse operation (22).

In Figure 7 we show performance plots for these routines and give in colors the relative error of λ_{14} for each computation. By drawing a vertical line in Figure 7 (a), it becomes clear that LU computation becomes more expensive for p -FEM than h -FEM. This is expected as matrices generated from p -FEM are denser than those from h -FEM. Moreover, from the plot we see that the TIAR performance is fairly balanced for both p -FEM and h -FEM depending mostly on N .

Regarding accuracy, we can draw a horizontal line in any of the plots in Figure 7 and pick two computations that lie close to this line, meaning that both took similar computational times. Then by comparing the errors given in colors, it is apparent that p -FEM reaches lower errors than

p	1	2	11	20
$ \lambda_j - \lambda_j^\gamma / \lambda_j $	10^{-4}	10^{-4}	10^{-4}	1.9×10^{-13}
N	1.4×10^6	22657	5697	141121
LU time (s)	440	3.23	0.47	228.73
TIAR time (s)	2464	18.58	4.74	149.05

Table 3: Comparison for fixed errors on λ_{14} in problem 5.2 with shift $\mu = 20 - 0.3i$.

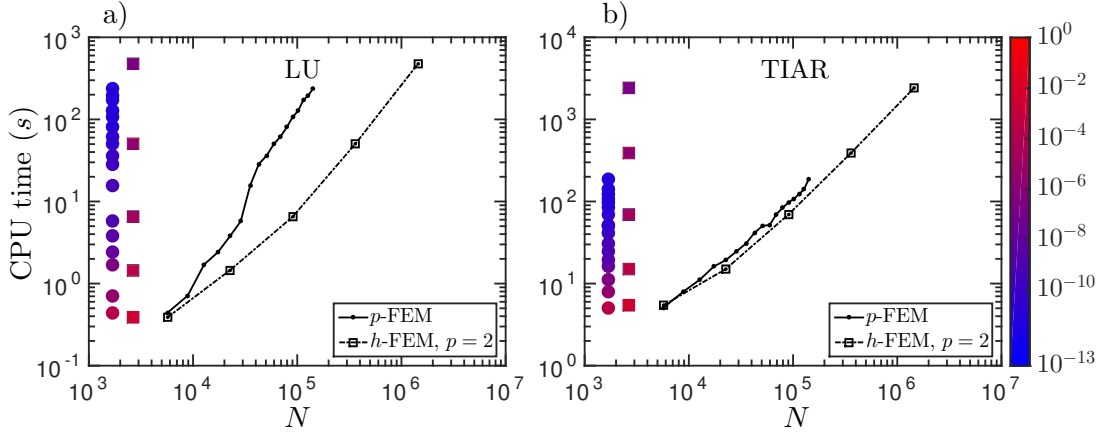


Figure 7: a) LU and b) TIAR performance for problem 5.2. In colors we give relative errors for p -FEM (bullets) and h -FEM (squares) computed for λ_{14} that correspond to the bullets/squares in black.

h -FEM for all computations. In Table 3 we list data for the numerical computation of λ_{14} and compare the performance for h -FEM and p -FEM by keeping accuracy fixed. The columns with $p = 1, 2$ are referred as h -FEM (low polynomial orders and several mesh refinements) and the column with $p = 11$ is p -FEM. In the last column ($p = 20$) we list data for a highly accurate p -FEM discretization. The simulations suggest that for the given problems 5.1 and 5.2 p -FEM surpasses h -FEM in terms of performance for the proposed NEP solver.

6. Conclusions and outlook

We have proposed a fast and efficient method for computing resonances and resonant modes of Helmholtz problems posed as a NEP. The finite element method is used for discretizing the problem, and the resulting NEP is solved with a new specialization of the infinite Arnoldi method. In the numerical experiments we observe that the performance of the TIAR iterations scale linearly with the problem size and it is stable with respect to the number of terms in the Dirichlet-to-Neumann map. A pole cancellation technique was successfully applied to increase the radius of convergence when the shift is close to a pole. The h and the p version of the finite element method were used to discretize the Fredholm operator function and we showed that the nonlinear matrix eigenvalue solver performs well in all cases. The exponential convergence of the p -version of FE, for problems with smooth interfaces, together with the new version of the infinite Arnoldi method is therefore an efficient tool for resonance calculations. Moreover, we expect the same performance for hp -FEM, since the sparsity of the matrices do not critically affect the performance of the TIAR

method.

Acknowledgments. We gratefully acknowledge the support of the Swedish Research Council under Grant No. 621-2012-3863 and 621-2013-4640. J. Araújo also thanks the department of Mathematics at KTH Royal Institute of Technology very much for the kind hospitality and Giampaolo Mele for interesting discussions held during the visit.

References

- [1] M. Abramowitz and I. A. Stegun, editors. *Handbook of Mathematical Functions*. Applied Mathematics Series No. 55. National Bureau of Standards, Washington D.C., 1970.
- [2] J. Asakura, T. Sakurai, H. Tadano, T. Ikegami, and K. Kimura. A numerical method for nonlinear eigenvalue problems using contour integrals. *JSIAM Letters*, 1:52–55, 2009.
- [3] I. Babuška and J. Osborn. Eigenvalue problems. In *Handbook of numerical analysis, Vol. II*, Handb. Numer. Anal., II, pages 641–787. North-Holland, Amsterdam, 1991.
- [4] I. Babuška, Q. Buo, and J. E. Osborn. Regularity and numerical solution of eigenvalue problems with piecewise analytic data. *SIAM J. Numer. Anal.*, 26(6):1534–1560, 1989.
- [5] I. Babuška and B. Q. Guo. The h, p and h-p version of the finite element method: Basis theory and applications. *Adv. Eng. Softw.*, 15(3-4):159–174, November 1992.
- [6] Satish Balay, William D. Gropp, Lois Curfman McInnes, and Barry F. Smith. Efficient management of parallelism in object oriented numerical software libraries. In E. Arge, A. M. Bruaset, and H. P. Langtangen, editors, *Modern Software Tools in Scientific Computing*, pages 163–202. Birkhäuser Press, 1997.
- [7] W. Bangerth, T. Heister, L. Heltai, G. Kanschat, M. Kronbichler, M. Maier, B. Turcksin, and T. D. Young. The **deal.II** library, version 8.2. *Archive of Numerical Software*, 3, 2015.
- [8] M. Van Barel and P. Kravanja. Nonlinear eigenvalue problems and contour integrals. *J. Comput. Appl. Math.*, 292:526–540, 2016.
- [9] R. Van Beeumen, K. Meerbergen, and W. Michiels. A rational Krylov method based on Hermite interpolation for nonlinear eigenvalue problems. *SIAM J. Sci. Comput.*, 35(1):A327–A350, 2013.
- [10] T. Betcke, N. J. Higham, V. Mehrmann, C. Schröder, and F. Tisseur. NLEVP: A collection of nonlinear eigenvalue problems. *ACM Trans. Math. Softw.*, 39(2):1–28, 2013.
- [11] T. Betcke and H. Voss. A Jacobi-Davidson type projection method for nonlinear eigenvalue problems. *Future Generation Computer Systems*, 20(3):363–372, 2004.
- [12] W.-J. Beyn. An integral method for solving nonlinear eigenvalue problems. *Linear Algebra Appl.*, 436(10):3839–3863, 2012.
- [13] Susanne C. Brenner and L. Ridgway Scott. *The mathematical theory of finite element methods*. Texts in applied mathematics. Springer, New York, Berlin, Paris, 2002.
- [14] P.G. Ciarlet and P.-A. Raviart. Interpolation theory over curved elements, with applications to finite element methods. *Computer Methods in Applied Mechanics and Engineering*, 1(2):217 – 249, 1972.
- [15] D. Colton and R. Kress. *Inverse Acoustic and Electromagnetic Scattering Theory*. Springer-Verlag, Berlin, 1992.
- [16] C. Dettmann, G. V. Morozov, M. Sieber, and H. Waalkens. Internal and external resonances of dielectric disks. *Europhysics letters*, 87(3), 2009.
- [17] C. P. Dettmann, G. V. Morozov, M. Sieber, and H. Waalkens. Internal and external resonances of dielectric disks. *EPL (Europhysics Letters)*, 87(3):34003, 2009.
- [18] Christian Engström and Luka Grubišić. A subspace iteration algorithm for Fredholm valued functions. *Math. Probl. Eng.*, pages Art. ID 459895, 14, 2015.
- [19] S. Fliss. A Dirichlet-to-Neumann approach for the exact computation of guided modes in photonic crystal waveguides. *SIAM J. Sci. Comput.*, 35(2):B438–B461, 2013.
- [20] I. C. Gohberg and M. G. Kreĭn. *Introduction to the theory of linear nonselfadjoint operators*, volume 18 of *Translations of mathematical monographs*. American Mathematical Society, Providence, Rhode Island, 1969.
- [21] S. Güttel, R. Van Beeumen, K. Meerbergen, and W. Michiels. NLEIGS: a class of fully rational Krylov methods for nonlinear eigenvalue problems. *SIAM J. Sci. Comput.*, 36(6):A2842–A2864, 2014.
- [22] Isaac Harari and Thomas J. R. Hughes. Analysis of continuous formulations underlying the computation of time-harmonic acoustics in exterior domains. *Comput. Methods Appl. Mech. Eng.*, 97(1):103–124, May 1992.
- [23] N. J. Higham. *Functions of Matrices. Theory and Computation*. SIAM, 2008.

- [24] A D Humphrey and W L Barnes. Plasmonic surface lattice resonances in arrays of metallic nanoparticle dimers. *Journal of Optics*, 18(3):035005, 2016.
- [25] T. Ikegami, T. Sakurai, and U. Nagashima. A filter diagonalization for generalized eigenvalue problems based on the Sakurai-Sugiura projection method. *J. Comput. Appl. Math.*, 233(8):1927–1936, 2010.
- [26] V. S. Ilchenko and A. B. Matsko. Optical resonators with whispering-gallery modes - Part II: Applications. *IEEE journal of selected topics in quantum electronics*, 12(1), January 2006.
- [27] E. Jarlebring, G. Mele, and O. Runborg. The waveguide eigenvalue problem and the tensor infinite Arnoldi method. Technical report, KTH Royal Institute of Technology, 2015. arxiv preprint.
- [28] E. Jarlebring, W. Michiels, and K. Meerbergen. A linear eigenvalue algorithm for the nonlinear eigenvalue problem. *Numer. Math.*, 122(1):169–195, 2012.
- [29] O. Karma. Approximation in eigenvalue problems for holomorphic Fredholm operator functions. I. *Numer. Funct. Anal. Optim.*, 17(3–4):365–387, 1996.
- [30] O. Karma. Approximation in eigenvalue problems for holomorphic Fredholm operator functions. II. *Numer. Funct. Anal. Optim.*, 17(3–4):389–408, 1996.
- [31] L. Kaufman. Eigenvalue problems in fiber optic design. *SIAM J. Matrix Anal. Appl.*, 28(1):105–117, 2006.
- [32] D. Klindworth and K. Schmidt. Dirichlet-to-Neumann transparent boundary conditions for photonic crystal waveguides. *IEEE Transactions on Magnetics*, 50(2):7005204, 2014.
- [33] D. Kressner. A block Newton method for nonlinear eigenvalue problems. *Numer. Math.*, 114(2):355–372, 2009.
- [34] M. Lenoir, M. Vullierme-Ledard, and C. Hazard. Variational formulations for the determination of resonant states in scattering problems. *SIAM J. Math. Anal.*, 23(3):579–608, 1992.
- [35] B.-S. Liao, Z. Bai, L.-Q. Lee, and K. Ko. Solving large scale nonlinear eigenvalue problems in next-generation accelerator design. Technical Report SLAC-PUB-12137, Stanford University, 2006.
- [36] B.-S. Liao, Z. Bai, L.-Q. Lee, and K. Ko. Nonlinear Rayleigh-Ritz iterative method for solving large scale nonlinear eigenvalue problems. *Taiwanese Journal of Mathematics*, 14(3):869–883, 2010.
- [37] Adi Ben-Israel Lily Yau. The newton and halley methods for complex roots. *The American Mathematical Monthly*, 105(9):806–818, 1998.
- [38] Richard B. Melrose. *Geometric scattering theory*. Stanford Lectures. Cambridge University Press, Cambridge, 1995.
- [39] N. Asger Mortensen, Søren Raza, Martijn Wubs, Thomas Søndergaard, and Sergey I. Bozhevolnyi. A generalized non-local optical response theory for plasmonic nanostructures. *Nature Communications*, 5, 2014.
- [40] Hae Soo Oh and Ivo Babuška. The p -version of the finite element method for the elliptic boundary value problems with interfaces. *Comput. Methods Appl. Mech. Engrg.*, 97(2):211–231, 1992.
- [41] G. Rosolen and B. Maes. Asymmetric and connected graphene dimers for a tunable plasmonic response. *Phys. Rev. B*, 92:205405, Nov 2015.
- [42] J. Sanchez Hubert and E. Sánchez-Palencia. *Vibration and coupling of continuous systems*. Springer-Verlag, Berlin, 1989. Asymptotic methods.
- [43] S. Sauter. hp -finite elements for elliptic eigenvalue problems: Error estimates which are explicit with respect to λ , h , and p . *SIAM J. Numer. Anal.*, 48(1):95–108, 2010.
- [44] C. Schwab. *p - and hp - Finite Element Methods: Theory and Applications in Solid and Fluid Mechanics*. Oxford University Press, 1998.
- [45] Pavel Solin, Karel Segeth, and Ivo Dolezel. *Higher-order finite element methods*. Studies in advanced mathematics. Chapman & Hall/CRC, Boca Raton, London, 2004.
- [46] A. Spence and C. Poulton. Photonic band structure calculations using nonlinear eigenvalue techniques. *J. Comput. Phys.*, 204(1):65–81, 2005.
- [47] D. B. Szyld and F. Xue. Preconditioned eigensolvers for large-scale nonlinear hermitian eigenproblems with variational characterization. I. conjugate gradient methods. Technical report, Temple University, 2014.
- [48] J. Tausch. Computing Floquet-Bloch modes in bi-periodic slabs with boundary elements. *J. Comput. Appl. Math.*, 254:192–203, 2013.
- [49] R. Van Beeumen. *Rational Krylov Methods for Nonlinear Eigenvalue Problems*. PhD thesis, Department of Computer Science, KU Leuven, Leuven, Belgium, 2015.
- [50] H. Voss. An Arnoldi method for nonlinear eigenvalue problems. *BIT*, 44:387 – 401, 2004.
- [51] H. Voss. Nonlinear eigenvalue problems. In L. Hogben, editor, *Handbook of Linear Algebra, Second Edition*, number 164 in Discrete Mathematics and Its Applications. Chapman and Hall/CRC, 2013.
- [52] G. N. Watson. *A treatise on the theory of Bessel functions*. Cambridge Mathematical Library. Cambridge University Press, Cambridge, 1995. Reprint of the second (1944) edition.
- [53] Maciej Zworski. Lectures on scattering resonances version 0.03. University Lecture, 2015.